Hindawi
Journal of Nanomaterials
Volume 2019, Article ID 3928526, 9 pages
https://doi.org/10.1155/2019/3928526

Research Article

Facile Synthesis of Yb^{3+}- and Er^{3+}-Codoped $LiGdF_4$ Colloidal Nanocrystals with High-Quality Upconversion Luminescence

Lu Zi,[1] Dan Zhang,[1] and Gejihu De [1,2,3]

[1]*College of Chemistry and Environment Science, Inner Mongolia Normal University, Hohhot 010022, China*
[2]*Physics and Chemistry of Functional Materials, Inner Mongolia Key Laboratory, Hohhot 010022, China*
[3]*State Key Laboratory on Integrated Optoelectronics, Jilin University, Changchun 130012, China*

Correspondence should be addressed to Gejihu De; degjh@imnu.edu.cn

Received 29 December 2018; Revised 14 March 2019; Accepted 14 April 2019; Published 16 May 2019

Academic Editor: Hiromasa Nishikiori

Herein, we synthesized high-quality colloidal nanocrystals of Yb^{3+}/Er^{3+}-codoped $LiGdF_4$ with intense green emission by using a facile route and turning the associated reaction parameters. Moreover, we probed the effects of reaction conditions on nanocrystal properties (crystal structure, morphology, and luminescence) and gained valuable mechanistic insights into nucleation and growth processes. Sample purity was found to depend on $LiOH{\cdot}H_2O$ concentration, reaction temperature, and time, which allowed us to manipulate sample purity and thus obtain species ranging from mixtures of $LiGdF_4$:Yb^{3+}/Er^{3+} with GdF_3 to pure tetragonal-phase $LiGdF_4$:Yb^{3+}/Er^{3+}. Investigation of upconversion luminescence properties and the luminescence lifetime of as-prepared samples revealed that $LiGdF_4$ is a promising host material for realizing the desired upconversion luminescence.

1. Introduction

Trivalent lanthanide ion- (Ln^{3+}-) doped nanocrystals, which can convert infrared radiation to visible luminescence, have attracted much attention in view of their excellent luminescence properties and unique application value [1–9]. The application fields are very wide including solid-state lasers, 3D displays, solar cells, photovoltaics, biological probe and label markers, and multimodal bioimaging [10–16]. Most of these nanocrystals correspond to fluorides, which exhibit several advantages over other halides, such as thermal and environmental stability, high refractive index, high transparency, low-frequency phonons, and lower emission threshold [17–20]. Among fluorides, those based on Gd^{3+} have been intensively researched because of their excellent chemical and optical properties [21–24]. Moreover, the energy gap between the $^6P_{7/2}$ and the $^8S_{7/2}$ levels of Gd^{3+} equals 32000 cm^{-1}, which allows Gd^{3+} to be used as an intermediary to promote fluoride energy transfer and thus greatly improve the efficiency of upconversion luminescence [25, 26].

Much research has been performed on the monodisperse, well-shaped, uniform-size, and phase-pure $NaGdF_4$ nanoparticles in recent decades [27–35]. For instance, Liu and coworkers prepared size-controllable, highly monodisperse, oleate-capped $NaGdF_4$:Yb,Er nanocrystals that can be used as biological probes for in vivo testing of tiny tumors [36], while Johnson's group showed that the regulation of reaction time and temperature allows the synthesis of size-tunable and ultrasmall $NaGdF_4$ nanoparticles (2.5-8.0 nm) [37]. There is no doubt that $NaGdF_4$ is considered to be an ideal rigid host matrix for upconversion, and its synthesis has therefore become a research hotspot for the majority of scholars. However, $LiGdF_4$ has been underexplored among the $AGdF_4$ ($A = Na^+, K^+, Li^+$) hosts because of the difficulty of synthesizing pure tetragonal-phase $LiGdF_4$ nanocrystals. To the best of our knowledge, $LiGdF_4$ nanocrystals are mainly prepared using Czochralski, sol-gel, or thermal decomposition methods. For instance, Cornacchia and coworkers prepared $LiGdF_4$:Tm^{3+} single crystals utilizing the Czochralski technique [38], while Lepoutre and coworkers prepared $90SiO_2 10LiGd_{1-x}Eu_xF_4$ ($x = 0$ or 0.05)

composites using a sol-gel method [39]. Moreover, Xiong's group successfully synthesized $LiGdF_4$ nanoparticles with different Ca^{2+} contents using a thermal decomposition method, revealing that Ca^{2+} ions are vital to the successful synthesis of these nanoparticles [40]. Na and coworkers prepared pure tetragonal-phase $LiGdF_4$ upconversion nanophosphors doped with Y^{3+} by thermal decomposition in a methanol-$LiOH{\cdot}H_2O$-NH_4F mixture and showed that the orthorhombic GdF_3 phase was produced at Y^{3+} doping degrees of 0-20 mol% [41]. Initially, we tried to prepare $LiGdF_4$:Yb,Er nanocrystals by similar methods of $LiYF_4$:Yb,Er nanocrystals used, while we did not get the result we wanted. After careful analysis, we speculate that it may be caused by various facts, such as chemical factor itself, equipment factor, and experimental environmental factor. Furthermore, we noted that the vast majority of $LiGdF_4$:Yb,Er nanocrystal syntheses employ solutions of oleic acid and 1-octadecenein methanol, which are highly toxic.

To address this challenge, we have developed a suitable synthetic route to prepare high-quality $LiGdF_4$:Yb/Er nanocrystals avoiding extra ion doping and the use of methanol-$LiOH{\cdot}H_2O$-NH_4F mixtures. An improved thermal decomposition method is introduced in this paper. Moreover, we determined optimal reaction conditions and investigated the influence of reaction temperature, reaction time, and $LiOH{\cdot}H_2O$ content on the upconversion luminescence properties and luminescence lifetimes.

2. Experimental

2.1. Materials. The synthesis was carried out using standard oxygen-free procedures and commercially available reagents. RE_2O_3 (RE = Gd^{3+} 99.95%, Yb^{3+} 99.99%, and Er^{3+} 99.99%), CF_3COOH (analytical grade 99.0%), oleic acid (OA, analytical grade), and $LiOH{\cdot}H_2O$ (>95.0%) were purchased from Sinopharm Chemical Reagent Beijing Co. Ltd. Absolute ethanol (analytical grade > 99.7%), cyclohexane (analytical grade 99.5%), and 1-octadecene (ODE, technical grade 90%) were purchased from Tianjin Chemical Co., Kemeng, and Sigma-Aldrich, respectively. All chemicals were used without further purification.

2.2. Synthesis of Precursor Mixture. We improved and modified previously reported methods to synthesize trifluoroacetate precursors [42–44]. Compared with the traditional preparation process of single trifluoroacetates of the lanthanides [$Ln(CF_3COO)_3$, Ln = Gd, Yb, and Er] and $Li(CF_3COO)_3$ samples, we are mixing the two to prepare precursor mixture. As for reaction vessel, we choose a 100 mL Teflon-lined autoclave to replace the traditional 100 mL three-neck flask. The process was carried out via adding Gd_2O_3 (0.78 mmol), Yb_2O_3 (0.2 mmol), Er_2O_3 (0.02 mmol), and a certain amount of $LiOH{\cdot}H_2O$ to the mixture solution of trifluoroacetic acid/water (6 mL : 6 mL). This turbid solution was vigorously stirred and transferred to a 100 mL Teflon-lined autoclave. Subsequently, the emulsion was heated and maintained at 80°C. After confinement for 12 h, the solution was cooled to room temperature and transferred to a 100 mL three-neck flask and dryly heated up at 60°C for evaporating excess CF_3COOH/H_2O. Then, the precursor mixture was obtained. The profit about such doing is that the preparation process will be safer and more convenient. It is mainly because a mixed solution of methanol, $LiOH{\cdot}H_2O$, and NH_4F for providing Li^+ or other doped ions is required in the traditional preparation process, while none of these is required in our preparation.

2.3. Synthesis of High-Quality Yb^{3+}/Er^{3+}-Codoped $LiGdF_4$ Colloidal Nanocrystals. The high-quality Yb^{3+}/Er^{3+}-codoped $LiGdF_4$ colloidal nanocrystals were prepared by a thermal decomposition route. The process was carried out via adding 15 mL OA and 15 mL ODE to precursor mixture. The cloudy solution was vigorously stirred to yield a transparent solution. Subsequently, the transparent solution was heated to 110°C under vacuum condition for removing needless water/oxygen. An hour later, the solution was heated to 310°C (or 280°C, 290°C, and 300°C) under an argon gas atmosphere and maintained for a period of time (1 h, 2 h, 3 h, 4 h, 5 h, or 6 h). The reaction system was cooled to room temperature and added excess absolute ethanol to precipitate products. The as-synthesized products were washed several times with cyclohexane/ethanol (1 : 4) mixed solution to remove the residue of organic ligands and other mixtures on the products and isolated by centrifugation at 8000 rpm for 3 min. Finally, the products were dried under vacuum to 60°C for 12 h to obtain a white powder sample for reserving.

3. Results and Discussions

3.1. Synthetic Procedure and Reaction Mechanism. Figure 1 illustrates the synthesis of high-quality Yb^{3+}/Er^{3+}-codoped $LiGdF_4$ colloidal nanocrystals, showing that it comprised two steps, namely, hydrothermal preparation of the precursor mixture, followed by thermal decomposition to afford $LiGdF_4$ colloidal nanocrystals.

To get better understanding, the nucleation and growth mechanisms of $LiGdF_4$:$Yb_{0.2}/Er_{0.02}$ colloidal nanocrystals are speculated in Scheme 1. Briefly, the process starts with the cothermolysis of $Gd(CF_3COO)_3$ and CF_3COOLi in oleic acid and 1-octadecene systems. When the reaction system is heated to 100~120°C, trifluoroacetate ligands are partially exchanged for oleic acid residues, and the C-F bond of the former is broken to release F^- when the reaction temperature further increases to 250~330°C. Subsequently, fluoride anions engage in fluorination and cleave Gd-$OOCCF_3$ bonds to promote nucleation, and the thus obtained crystal nuclei agglomerate to form larger particles as the reaction progresses. With the increase of temperature, the growth rate of these nuclei crystal nucleus increases and eventually forms nanocrystals [45–48].

3.2. Structure and Morphology. Sample crystal structures were characterized by using a Rigaku Ultima IV X-ray diffractometer with Cu Kα radiation ($\lambda = 0.15406$ nm) at 200 mA and 40 kV. XRD patterns were recorded for dried powders in the range of $2\theta = 15°$~$80°$ at a step size of 8°/min. Figure 2 clearly demonstrates the growth kinetics of

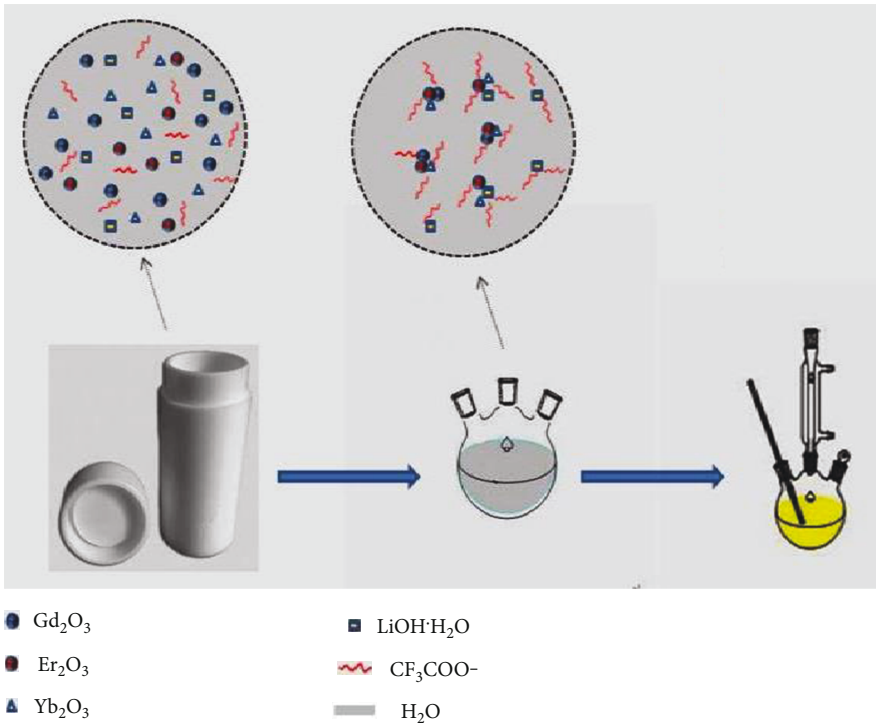

Figure 1: Synthesis of $LiGdF_4:Yb^{3+}/Er^{3+}$ colloidal nanocrystals.

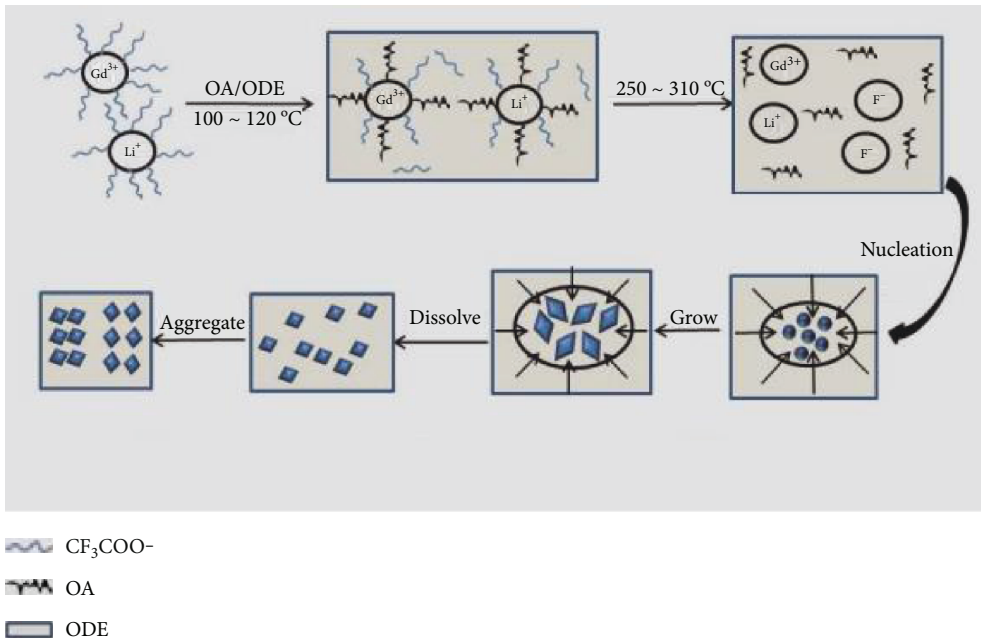

Scheme 1: Schematic of the reaction mechanism.

$LiGdF_4:Yb^{3+}/Er^{3+}$ nanocrystals synthesized at different reaction times. It is not hard to find that the diffraction peaks of samples obtained at $Li^+/Gd^{3+} = 3$ and $t = 1$ h, 2 h, and 3 h corresponded to a mixture of $LiGdF_4$ (JCPDS No. 27-1236) and GdF_3 (JCPDS No. 49-1804), whereas those obtained at $Li^+/Gd^{3+} = 3$ and $t = 4$ h and 5 h contain $LiGdF_4$ (JCPDS No. 27-1236). Hence, 4 or 5 h was concluded to be the optimal reaction times for synthesizing $LiGdF_4:Yb^{3+}/Er^{3+}$ nanocrystals.

Next, we studied the optimum reaction temperature for preparing $LiGdF_4:Yb^{3+}/Er^{3+}$ colloidal nanocrystals. Figure 3 clearly demonstrates the formation of $LiGdF_4$ with GdF_3 at $Li^+/Gd^{3+} = 3$ and temperatures (T) of 280, 290, and 300°C, revealing that $LiGdF_4$ nuclei were instantly formed

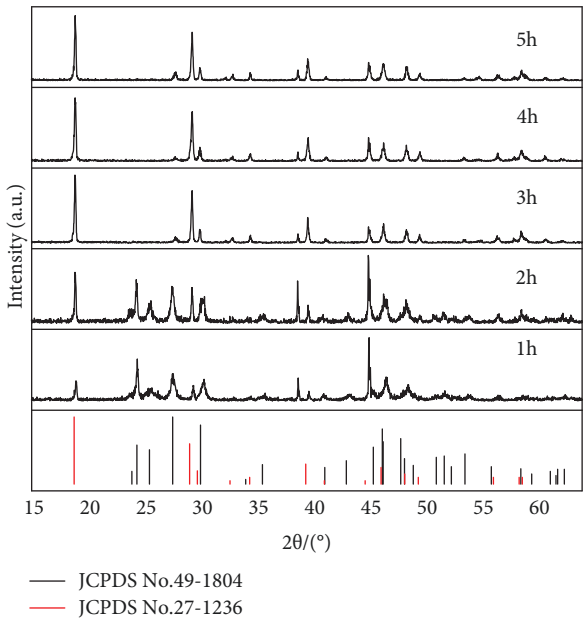

FIGURE 2: XRD patterns of $LiGdF_4$:Yb^{3+}/Er^{3+} colloidal nanocrystals, which are synthesized at $Li^+/Gd^{3+} = 3$ and $t = 1$ h, 2 h, 3 h, 4 h, and 5 h.

even at 280°C and that the growth rate of these nuclei increased with the increasing temperature. A balance between nucleation and growth was established at 310°C, which was concluded to be the optimum reaction temperature for the synthesized tetragonal $LiGdF_4$:Yb^{3+}/Er^{3+} nanocrystals. Finally, the optimum Li/RE ratio was determined as three, although the optimization of Li^+ concentration proved to be very tortuous. Details of the synthetic process and parameters of tetragonal-phase $LiGdF_4$:Yb^{3+}/Er^{3+} colloidal nanocrystals are given in the supporting information (Figure S1, S2, and Table S1). Thus, the above experimental results suggest that the optimum conditions for tetragonal $LiGdF_4$:Yb^{3+}/Er^{3+} nanocrystal synthesis were determined as $Li^+/Gd^{3+} = 3$, $t = 4$ h, and $T = 310$°C (Table S1).

Sample morphology was assessed by transmission electron microscopy (TEM) and high-resolution transmission electron microscopy (HRTEM) with a FEI Tecnai G2 F20 S-Twin transmission electron microscope operating at 200 kV. Samples for TEM imaging were prepared by drying nanocrystal dispersions in cyclohexane on amorphous carbon-coated Cu grids. Representative TEM micrographs of as-synthesized $LiGdF_4$ nanocrystals (relatively pure tetragonal phase) are displayed in Figure 4. Figures 4(a)–4(d) show low-magnification TEM images, while Figures 5(a) and 5(b) show high-magnification TEM images with related selected-area electron diffraction patterns, revealing that the as-synthesized $LiGdF_4$:Yb^{3+}/Er^{3+} nanocrystals can withstand irradiation with high-energy electrons. From the TEM images, we can also see that most of the samples are octahedron and sphere. And the average sizes of these crystals focus on 137.7 nm nearby in Figure 4(e), while the octahedral crystals focus on 98 nm length × 98 nm length × 18 nm thickness on average. HRTEM imaging revealed the presence of obvious lattice fringes, indicating the high crystallinity of individual particles. The adjacent lattice spacing calculated by FFT analysis (~0.47 nm) was assigned to the (101) crystal plane of tetragonal-phase $LiGdF_4$, which confirmed that as-synthesized $LiGdF_4$ nanocrystals exhibited high crystallinity and few defects.

3.3. Upconversion Luminescence. Upconversion emission spectra were recorded on a Hitachi F-4600 fluorescence spectrophotometer (slit width = 5.0 nm, PMT voltage = 700 V, and $\lambda = 400 - 700$ nm) under excitation with an adjustable 980 nm NIR laser diode. Room temperature upconversion emission spectra are obtained by drying the nanocrystal dispersion in cyclohexane at a concentration of 2 mg/mL. It is formed into a colloidal solution by dispersing dried powder in cyclohexane for several hours' ultrasound.

It is well known that Yb^{3+}- and Er^{3+}-codoped rare earth fluorides can exhibit strong upconversion luminescence upon 980 nm near-infrared excitation, as observed herein for the colloidal suspension of $LiGdF_4$:Yb^{3+}/Er^{3+}. Two visible-light-region emission bands, positioned at 523 and 543 nm (green upconversion luminescence) and 672 nm (red upconversion luminescence), were observed for all samples in Figures 6(a) and 6(b). The above bands were ascribed to $^2H_{11/2} \rightarrow {}^4I_{15/2}$, $^4S_{3/2} \rightarrow {}^4I_{15/2}$, and $^4F_{9/2} \rightarrow {}^4I_{15/2}$ transitions, respectively. Meanwhile, we also find that the intensity of upconversion luminescence increased with increasing reaction time, which was mainly attributed to the concomitant increase of tetragonal phase content. This phase could be obtained in relatively pure form at $Li^+/Gd^{3+} = 3$, $t = 4$ h, and $T = 310$°C, while mixtures of $LiGdF_4$ with GdF_3, exhibiting lower upconversion luminescence intensities because of the presence of the latter component and other impurities, were obtained otherwise. It is surprising that there is a sudden drop in the upconversion luminescence intensity of the sample, which is synthesized at $Li^+/Gd^{3+} = 3$, $t = 5$ h, and $T = 310$°C. This finding might be attributed to the fact that the content of GdF_3 and other impurities in the above sample exceeded that in the optimal condition sample.

In addition, it might be that the growth rate of $LiGdF_4$ crystal nucleus reached the maximum at 4 h, while the reaction time that further increased to 5 h might lead to excessive surfactant and activator ions accumulate on the crystal surface. All of these cause fluorescence quenching of the sample, which is synthesized at $Li^+/Gd^{3+} = 3$, $t = 5$ h, and $T = 310$°C. The clear contrast figures of emission intensity and reaction time are provided in the supporting information (Figure S3 and Table S2). To gain further insights into the upconversion emission process, we investigated the dependence of upconversion emission intensity on excitation power adopting the $\log I_{em} \propto \log I^n_{ex}$ relation for data analysis in Figure 6(c). We regard the tetragonal $LiGdF_4$ nanocrystals as example to illuminate the upconversion emission process. The slopes of Gaussian function-based log-log fits were determined as 2.11 and 1.95 for the dominant green emissions at 523 and 543 nm, respectively, which illustrated that these emissions involve a

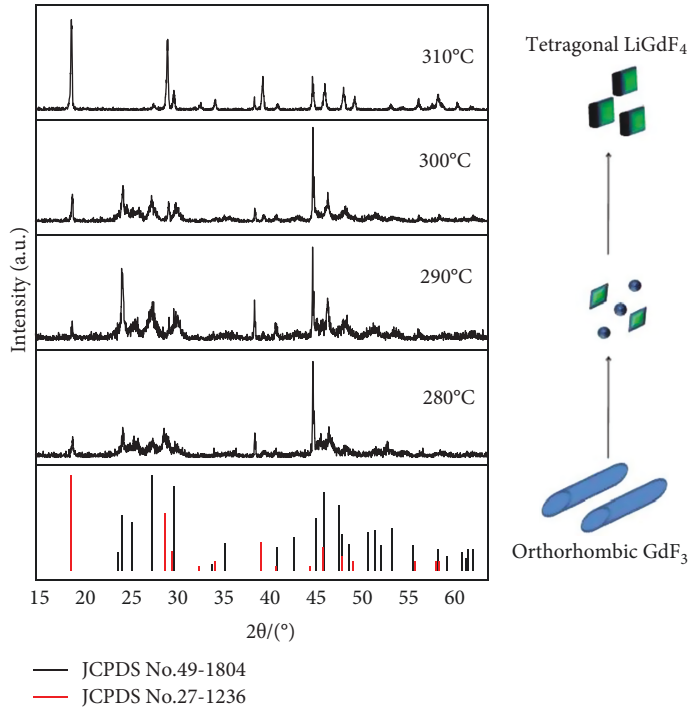

FIGURE 3: XRD patterns of $LiGdF_4$:Yb^{3+}/Er^{3+} colloidal nanocrystals, which are synthesized at $Li^+/Gd^{3+} = 3$ and $T = 280°C$, 290°C, 300°C, and 310°C.

two-photon process. For red emission, the corresponding slope was obtained as 2.37, and the same conclusion was drawn. It corresponds with the analysis of upconversion emissions mechanism.

Figure 7 schematically illustrates energy transfer and upconversion emission processes occurring at an excitation wavelength of 980 nm and a pump power density of 55 mW/cm^2. Under continuous excitation at 980 nm photon, sensitizer Yb^{3+} ions can be excited from the $^2F_{7/2}$ ground state to the $^2F_{5/2}$ state. Subsequently, the latter states decay back to the former, and the released energy is captured by nearby Er^{3+} ions, which are excited from the $^4I_{15/2}$ ground state into the $^4I_{11/2}$ state. Further energy capture by Er^{3+} ions in the $^4I_{11/2}$ excited state results in the population of a higher-lying $^4F_{7/2}$ state that can relax to the $^2H_{11/2}$ and $^4S_{3/2}$ levels (nonradiatively) and to the $^4I_{15/2}$ level (radiatively) with dominant $^2H_{11/2} \rightarrow {}^4I_{15/2}$ and $^4S_{3/2} \rightarrow {}^4I_{15/2}$ transitions resulting in green emission. Alternatively, Er^{3+} ions in the $^4I_{11/2}$ excited state can nonradiatively relax to the $^4I_{13/2}$ state and capture further energy to populate a higher-lying $^4F_{9/2}$ state that subsequently radiatively relaxes to the $^4I_{15/2}$ level with dominant $^4F_{9/2} \rightarrow {}^4I_{15/2}$ transitions resulting in red emissions. Notably, as-synthesized $LiGdF_4$ nanocrystals not only showed higher upconversion emission intensity but also longer luminescence lifetime (Figure 8 and Figure S4).

The decay of upconversion luminescence was recorded at room temperature using a lifetime fluorescence spectrometer (Delta Flex TCSPC system, Horiba Scientific, Scotland) equipped with an adjustable pulse laser as excitation source (slit width = 16 nm, wavelength = 980 nm, pulse width = 100 ns, and output power = 100 Hz). The obtained decay curves were fitted by a single-exponential function, and the effective UCL lifetime of nonexponential decay was calculated as

$$\tau_{\text{eff}} = \frac{1}{I_{\max}} \int_0^{\infty} I(t)dt, \quad (1)$$

where $I_{\max}$ is the maximum upconversion luminescence intensity and $I(t)$ is the upconversion luminescence intensity as a function of time [49, 50]. The UCL lifetimes of the $^2H_{11/2}$ state, determined by monitoring Er^{3+} emission at 523 nm under 980 nm, were found to increase with a reaction time of up to 4 h, equalling 369.30 (2 h), 663.23 (3 h), 745.74 μs (4 h), and 540.45 μs (5 h), respectively (Figure 8). This result confirmed that the sample synthesized at $Li^+/Gd^{3+} = 3$, $t =$ 4 h, and $T = 310°C$ exhibited good photostability because of the relatively pure tetragonal phase. In other samples, the presence of impurity ingredients led to the rapid migration of energy to lattice defects or surface quenchers, inducing luminescence quenching. This behaviour was consistent with the trend of upconversion emission intensity in Figure 6(a). Finally, we measured the lifetimes of $^2H_{11/2}$, $^4S_{3/2}$, and $^4F_{9/2}$ states of Er^{3+} under 980 nm excitation in $LiGdF_4$:Yb^{3+}/Er^{3+} nanocrystals, synthesized at $Li^+/Gd^{3+} = 3$, $t = 4$ h, and $T = 310°C$ (Figure S4), revealing increases from 663.23 μs (523 nm) and 665.54 μs (543 nm) to 678.41 μs (672 nm), respectively.

4. Conclusion

We have successfully improved and modified previously reported methods to synthesize high-quality Yb^{3+}/Er^{3+}-

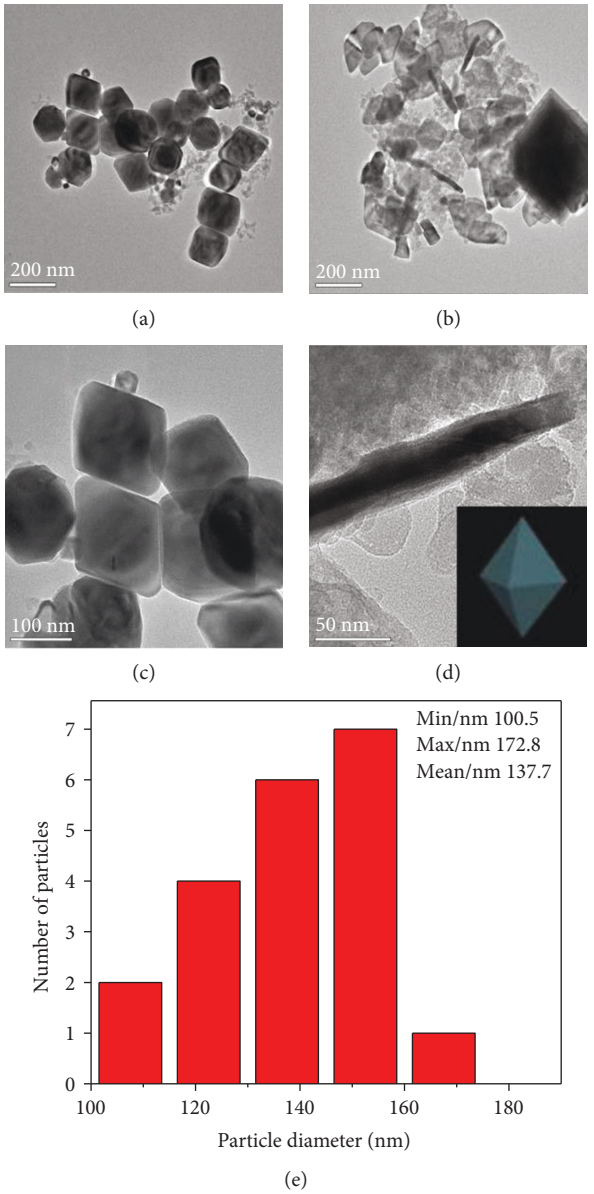

Figure 4: (a–d) TEM images of $LiGdF_4:Yb^{3+}/Er^{3+}$ nanocrystals, which are synthesized at $Li^+/Gd^{3+} = 3$, $t = 4$ h, and $T = 310°C$. (e) Grain size distribution histograms of Figure 4(a).

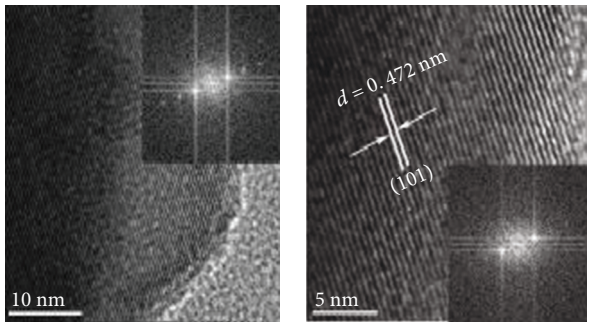

Figure 5: HRTEM images of $LiGdF_4:Yb^{3+}/Er^{3+}$ nanocrystals, which are synthesized at $Li^+/Gd^{3+} = 3$, $t = 4$ h, and $T = 310°C$. The insets of (a) and (b) correspond with Fourier transform electron diffraction pattern.

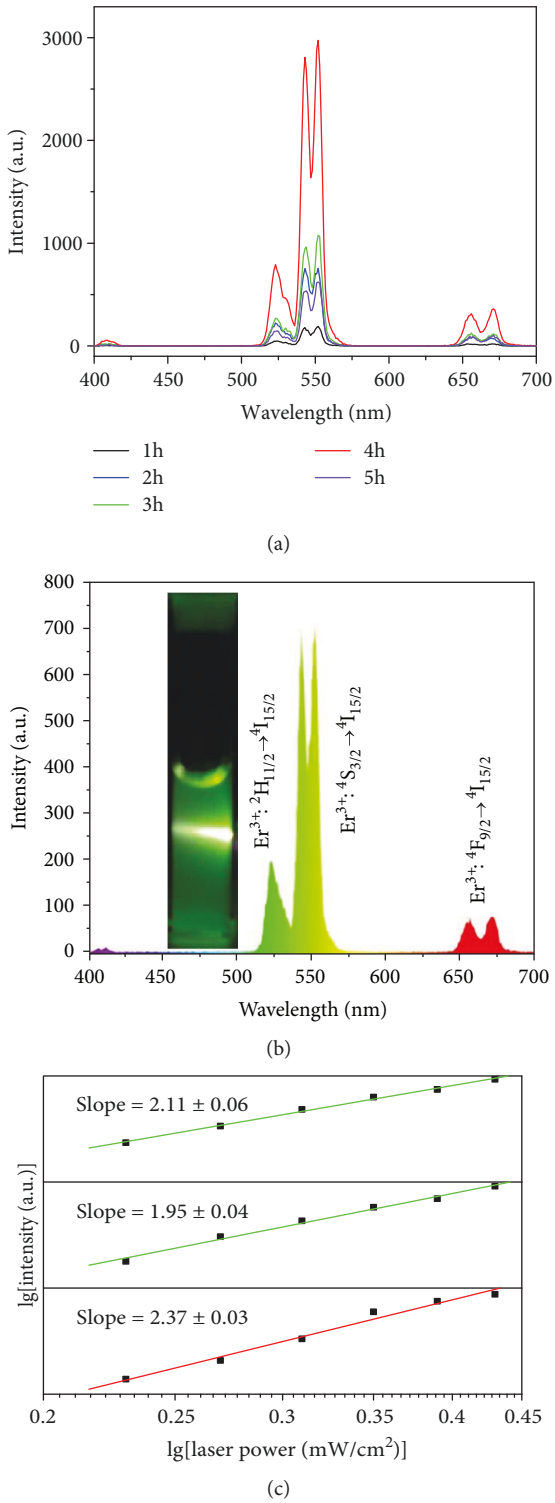

Figure 6: (a) Room temperature upconversion emission spectra of $LiGdF_4$:Yb^{3+}/Er^{3+} nanocrystals, which are synthesized at $Li^+/Gd^{3+} = 3$ and $t = 1$ h, 2 h, 3 h, 4 h, and 5 h. (b) Room temperature upconversion emission spectra of $LiGdF_4$:Yb^{3+}/Er^{3+} nanocrystals, which are synthesized at $Li^+/Gd^{3+} = 3$, $t = 4$ h, and $T = 310$°C. (c) Log-log plot of power dependence of the upconversion emissions intensity for $LiGdF_4$:Yb^{3+}/Er^{3+} nanocrystals at $Li^+/Gd^{3+} = 3$, $t = 4$ h, and $T = 310$°C.

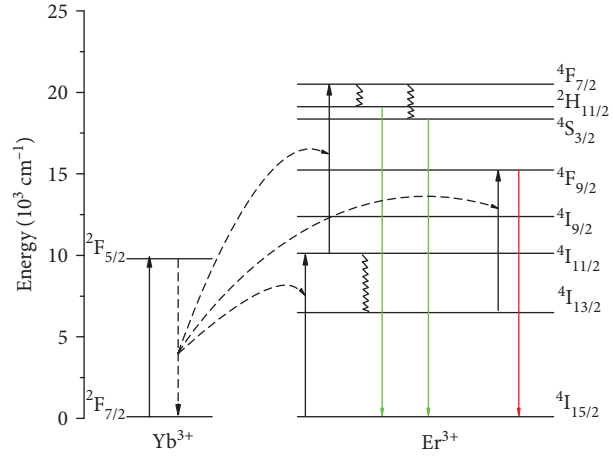

Figure 7: Energy level diagrams of upconversion emissions from Yb^{3+} to Er^{3+} in $LiGdF_4$:Yb^{3+}/Er^{3+} nanocrystals under 980 nm pump power excitation.

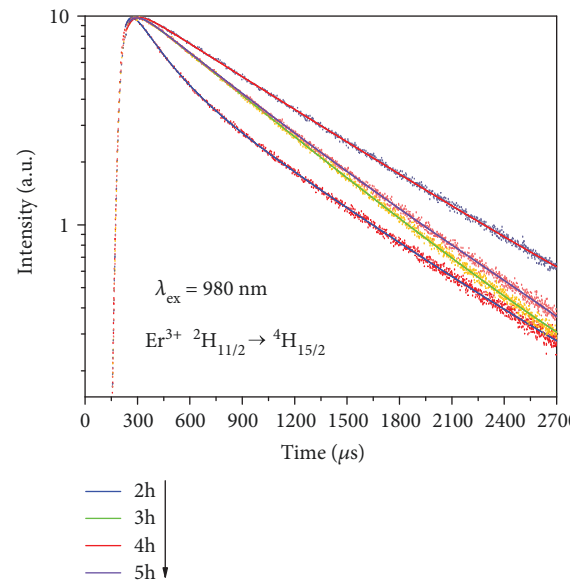

Figure 8: UCL decays from $^2H_{11/2}$ of Er^{3+} by monitoring the Er^{3+} emission at 523 nm under 980 nm excitation in $LiGdF_4$:Yb^{3+}/Er^{3+} nanocrystals, which are synthesized at $Li^+/Gd^{3+} = 3$, $T = 310$°C, and $t = 2$ h, 3 h, 4 h, and 5 h.

codoped $LiGdF_4$ colloidal nanocrystals with intense green emission. Specifically, the above synthesis involved the hydrothermal preparation of trifluoroacetate precursors $Gd(CF_3COO)_3$ and CF_3COOLi that were subsequently thermolyzed to afford the desired nanocrystals. Importantly, the adopted approach obviated the need for additional ion doping and the use of toxic methanol-$LiOH{\cdot}H_2O$-NH_4F mixture. Studies on the impact of $LiOH{\cdot}H_2O$ concentration, reaction temperature, and time on the upconversion luminescence of nanocrystal samples showed that relatively phase-pure tetragonal $LiGdF_4$ nanocrystals could be obtained under optimal conditions ($Li^+/Gd^{3+} = 3$, $t = 4$ h, and $T = 310$°C). Moreover, as-synthesized $LiGdF_4$:Yb^{3+}/Er^{3+} nanocrystals

not only showed a stronger upconversion emission intensity but also featured a longer luminescence lifetime. This work paves the way to the broad utilization of $LiGdF_4$, which is viewed as an ideal alternative matrix material, since the ionic radius of Li^+ is much smaller than that of Na^+. Herein, this research work will be indispensable for further follow-up study.

Data Availability

All data are obtained through our own experiments. The public database is not used in this article. If the reader needs the data in this article, he can contact the corresponding author.

Conflicts of Interest

The authors declare that they have no conflict of interest.

Acknowledgments

We gratefully acknowledge professor Gejihu De for guiding and the testing Center of Inner Mongolia University. This work is supported by the Postgraduate Scientific Research Innovation Foundation of Inner Mongolia University (Grant No. CXJJS15082), Open Fund of the State Key Laboratory on Integrated Optoelectronics (Grant No. IOSKL2013KF08), National Science Foundation of China (Grant No. 21261016), and Talents Project Inner Mongolia of China (Grant No. CYYC5026).

Supplementary Materials

Supplementary material including X-ray diffraction patterns of as-prepared samples, decay curves of $LiGdF_4$:Yb^{3+}/Er^{3+} nanocrystals, and discussion of influencing factors (such as temperature, time, and emission intensity). *(Supplementary Materials)*

References

[1] Z. L. Wang, H. L. W. Chan, H. L. Li, and J. H. Hao, "Highly efficient low-voltage cathodoluminescence of LaF_3:Ln^{3+} (Ln=Eu^{3+},Ce^{3+},Tb^{3+}) spherical particles," *Applied Physics Letters*, vol. 93, no. 14, article 141106, 2008.

[2] F. Zhang and D. Zhao, "Fabrication of ordered magnetite-doped rare earth fluoride nanotube arrays by nanocrystal self-assembly," *Nano Research*, vol. 2, no. 4, pp. 292–305, 2009.

[3] S. Fan, S. Wang, W. Xu, M. Li, H. Sun, and L. Hu, "Enormously enhanced upconversion emission in β-$NaYF_4$:20Yb,2Er microcrystals via Na^+ ion exchange," *Journal of Materials Science*, vol. 52, no. 2, pp. 869–877, 2017.

[4] F. Vetrone, R. Naccache, A. Zamarrón et al., "Temperature sensing using fluorescent nanothermometers," *ACS Nano*, vol. 4, no. 6, pp. 3254–3258, 2010.

[5] V. Mahalingam, F. Mangiarini, F. Vetrone et al., "Bright white upconversion emission from Tm^{3+}/Yb^{3+}/Er^{3+}-doped $Lu_3Ga_5O_{12}$ nanocrystals," *The Journal of Physical Chemistry C*, vol. 112, no. 46, pp. 17745–17749, 2008.

[6] X. Zou, M. Xu, W. Yuan et al., "A water-dispersible dye-sensitized upconversion nanocomposite modified with phosphatidylcholine for lymphatic imaging," *Chemical Communications*, vol. 52, no. 91, pp. 13389–13392, 2016.

[7] W. Yang, X. Li, D. Chi, H. Zhang, and X. Liu, "Lanthanide-doped upconversion materials: emerging applications for photovoltaics and photocatalysis," *Nanotechnology*, vol. 25, no. 48, article 482001, 2014.

[8] C. Zhang, H. P. Zhou, L. Y. Liao et al., "Luminescence modulation of ordered upconversion nanopatterns by a photochromic diarylethene: rewritable optical storage with nondestructive readout," *Advanced Materials*, vol. 22, no. 5, pp. 633–637, 2010.

[9] T. Zako, H. Nagata, N. Terada, M. Sakono, K. Soga, and M. Maeda, "Improvement of dispersion stability and characterization of upconversion nanophosphors covalently modified with PEG as a fluorescence bioimaging probe," *Journal of Materials Science*, vol. 43, no. 15, pp. 5325–5330, 2008.

[10] F. Wang and X. Liu, "Recent advances in the chemistry of lanthanide-doped upconversion nanocrystals," *Chemical Society Reviews*, vol. 38, no. 4, pp. 976–989, 2009.

[11] H. Guo, Z. Li, H. Qian, Y. Hu, and I. N. Muhammad, "Seed-mediated synthesis of NaY F_4:Y b, Er/$NaGdF_4$ nanocrystals with improved upconversion fluorescence and MR relaxivity," *Nanotechnology*, vol. 21, no. 12, article 125602, 2010.

[12] S. V. Eliseeva and J. C. G. Bünzli, "Lanthanide luminescence for functional materials and bio-sciences," *Chemical Society Reviews*, vol. 39, no. 1, pp. 189–227, 2010.

[13] B. M. Tissue, "Synthesis and luminescence of lanthanide ions in nanoscale insulating hosts," *Chemistry of Materials*, vol. 10, no. 10, pp. 2837–2845, 1998.

[14] J. Kim, Y. Piao, and T. Hyeon, "Multifunctional nanostructured materials for multimodal imaging, and simultaneous imaging and therapy," *Chemical Society Reviews*, vol. 38, no. 2, pp. 372–390, 2009.

[15] X. Liu, X. Kong, Y. Zhang et al., "Breakthrough in concentration quenching threshold of upconversion luminescence *via* spatial separation of the emitter doping area for bio-applications," *Chemical Communications*, vol. 47, no. 43, pp. 11957–11959, 2011.

[16] Y. Liu, Y. Chen, Y. Lin, Q. Tan, Z. Luo, and Y. Huang, "Energy transfer in Yb^{3+}–Er^{3+}-codoped bismuth borate glasses," *Journal of the Optical Society of America B*, vol. 24, no. 5, pp. 1046–1052, 2007.

[17] F. Wang, J. Wang, J. Xu, X. Xue, H. Chen, and X. Liu, "Tunable upconversion emissions from lanthanide-doped monodisperse β-$NaYF_4$ nanoparticles," *Spectroscopy Letters*, vol. 43, no. 5, pp. 400–405, 2010.

[18] E. van der Kolk, P. Dorenbos, K. Krämer, D. Biner, and H. U. Güdel, "High-resolution luminescence spectroscopy study of down-conversion routes in$NaGdF_4$:Nd^{3+} and $NaGdF_4$:Tm^{3+} using synchrotron radiation," *Physical Review B*, vol. 77, no. 12, article 125110, 2008.

[19] C. Li and J. Lin, "Rare earth fluoride nano-/microcrystals: synthesis, surface modification and application," *Journal of Materials Chemistry*, vol. 20, no. 33, pp. 6831–6847, 2010.

[20] P. R. Diamente, M. Raudsepp, and F. C. J. M. van Veggel, "Dispersible Tm^{3+}-doped nanoparticles that exhibit strong 1.47 μm photoluminescence," *Advanced Functional Materials*, vol. 17, no. 3, pp. 363–368, 2007.

[21] R. T. Wegh, H. Donker, K. D. Oskam, and A. Meijerink, "Visible quantum cutting in $LiGdF_4:Eu^{3+}$ through downconversion," *Science*, vol. 283, no. 5402, pp. 663–666, 1999.

[22] F. You, S. Huang, S. Liu, and Y. Tao, "VUV excited luminescence of $MGdF_4:Eu^{3+}$ (M=Na, K, NH_4)," *Journal of Luminescence*, vol. 110, no. 3, pp. 95–99, 2004.

[23] R. Naccache, F. Vetrone, V. Mahalingam, L. A. Cuccia, and J. A. Capobianco, "Controlled synthesis and water dispersibility of hexagonal phase $NaGdF_4:Ho^{3+}/Yb^{3+}$ nanoparticles," *Chemistry of Materials*, vol. 21, no. 4, pp. 717–723, 2009.

[24] T. Li, S. Liu, H. Zhang, E. Wang, L. Song, and P. Wang, "Ultraviolet upconversion luminescence in $Y_2O_3:Yb^{3+},Tm^{3+}$ nanocrystals and its application in photocatalysis," *Journal of Materials Science*, vol. 46, no. 9, pp. 2882–2886, 2011.

[25] Y. Wu, C. Li, D. Yang, and J. Lin, "Rare earth β-$NaGdF_4$ fluorides with multiform morphologies: hydrothermal synthesis and luminescent properties," *Journal of Colloid and Interface Science*, vol. 354, no. 2, pp. 429–436, 2011.

[26] H. Dong, L. D. Sun, and C. H. Yan, "Energy transfer in lanthanide upconversion studies for extended optical applications," *Chemical Society Reviews*, vol. 44, no. 6, pp. 1608–1634, 2015.

[27] C. De Nadaï, A. Demourgues, L. Lozano, P. Gravereau, and J. Grannec, "Structural investigations of new copper fluorides $NaRECu_2F_8$ (RE^{3+}=Sm^{3+}, Eu^{3+}, Gd^{3+}, Y^{3+}, Er^{3+}, Yb^{3+})," *Journal of Materials Chemistry*, vol. 8, no. 11, pp. 2487–2491, 1998.

[28] H. X. Mai, Y. W. Zhang, R. Si et al., "High-quality sodium rare-earth fluoride nanocrystals: controlled synthesis and optical properties," *Journal of the American Chemical Society*, vol. 128, no. 19, pp. 6426–6436, 2006.

[29] J. Y. Park, M. J. Baek, E. S. Choi et al., "Paramagnetic ultrasmall gadolinium oxide nanoparticles as advanced T_1 MRI contrast agent: account for large longitudinal relaxivity, optimal particle diameter, and *in vivo* T_1 MR images," *ACS Nano*, vol. 3, no. 11, pp. 3663–3669, 2009.

[30] R. Naccache, P. Chevallier, J. Lagueux et al., "High relaxivities and strong vascular signal enhancement for $NaGdF_4$ nanoparticles designed for dual MR/optical imaging," *Advanced Healthcare Materials*, vol. 2, no. 11, pp. 1478–1488, 2013.

[31] R. Lv, S. Gai, Y. Dai, N. Niu, F. He, and P. Yang, "Highly uniform hollow GdF_3 spheres: controllable synthesis, tuned luminescence, and drug-release properties," *ACS Applied Materials & Interfaces*, vol. 5, no. 21, pp. 10806–10818, 2013.

[32] H. Chen, X. Li, F. Liu, H. Zhang, and Z. Wang, "Renal clearable peptide functionalized $NaGdF_4$ nanodots for high-efficiency tracking orthotopic colorectal tumor in mouse," *Molecular Pharmaceutics*, vol. 14, no. 9, pp. 3134–3141, 2017.

[33] M. Ahrén, L. Selegård, A. Klasson et al., "Synthesis and characterization of PEGylated Gd_2O_3 nanoparticles for MRI contrast enhancement," *Langmuir*, vol. 26, no. 8, pp. 5753–5762, 2010.

[34] S. Dühnen, T. Rinkel, and M. Haase, "Size control of nearly monodisperse β-$NaGdF_4$ particles prepared from small α-$NaGdF_4$ nanocrystals," *Chemistry of Materials*, vol. 27, no. 11, pp. 4033–4039, 2015.

[35] J. L. Bridot, A. C. Faure, S. Laurent et al., "Hybrid gadolinium oxide nanoparticles: multimodal contrast agents for in vivo imaging," *Journal of the American Chemical Society*, vol. 129, no. 16, pp. 5076–5084, 2007.

[36] C. Liu, Z. Gao, J. Zeng et al., "Magnetic/upconversion fluorescent $NaGdF_4$:Yb,Er nanoparticle-based dual-modal molecular probes for imaging tiny tumors *in vivo*," *ACS Nano*, vol. 7, no. 8, pp. 7227–7240, 2013.

[37] N. J. J. Johnson, W. Oakden, G. J. Stanisz, R. Scott Prosser, and F. C. J. M. van Veggel, "Size-tunable, ultrasmall $NaGdF_4$ nanoparticles: insights into their T_1 MRI contrast enhancement," *Chemistry of Materials*, vol. 23, no. 16, pp. 3714–3722, 2011.

[38] F. Cornacchia, A. Di Lieto, and M. Tonelli, "$LiGdF_4:Tm^{3+}$: spectroscopy and diode-pumped laser experiments," *Applied Physics B*, vol. 96, no. 2-3, pp. 363–368, 2009.

[39] S. Lepoutre, D. Boyer, S. Fujihara, and R. Mahiou, "Structural and optical characterizations of sol–gel based composites constituted of $LiGdF_4:Eu^{3+}$ nanocrystallites dispersed into a silica matrix," *Journal of Materials Chemistry*, vol. 19, no. 18, pp. 2784–2788, 2009.

[40] Z. Xiong, Y. Yang, and Y. Wang, "Enhanced upconversion luminescence and tuned red-to-green emission ratio of $LiGdF_4$ nanocrystals *via* Ca^{2+} doping," *RSC Advances*, vol. 6, no. 79, pp. 75664–75668, 2016.

[41] H. Na, J. S. Jeong, H. J. Chang et al., "Facile synthesis of intense green light emitting $LiGdF_4$:Yb,Er-based upconversion bipyramidal nanocrystals and their polymer composites," *Nanoscale*, vol. 6, no. 13, pp. 7461–7468, 2014.

[42] G. S. Yi, W. B. Lee, and G. M. Chow, "Synthesis of $LiYF_4$, $BaYF_5$, and $NaLaF_4$ optical nanocrystals," *Journal of Nanoscience and Nanotechnology*, vol. 7, no. 8, pp. 2790–2794, 2007.

[43] H. T. Wong, F. Vetrone, R. Naccache, H. L. W. Chan, J. Hao, and J. A. Capobianco, "Water dispersible ultrasmall multifunctional $KGdF_4:Tm^{3+}$, Yb^{3+} nanoparticles with near-infrared to near-infrared upconversion," *Journal of Materials Science*, vol. 21, no. 41, pp. 16589–16596, 2011.

[44] Q. Cheng, J. Sui, and W. Cai, "Enhanced upconversion emission in Yb^{3+} and Er^{3+} codoped $NaGdF_4$ nanocrystals by introducing Li^+ ions," *Nanoscale*, vol. 4, no. 3, pp. 779–784, 2012.

[45] M. Li, H. Schnablegger, and S. Mann, "Coupled synthesis and self-assembly of nanoparticles to give structures with controlled organization," *Nature*, vol. 402, no. 6760, pp. 393–395, 1999.

[46] J. Shin, J. H. Kyhm, A. R. Hong et al., "Multicolor tunable upconversion luminescence from sensitized seed-mediated grown $LiGdF_4$:Yb,Tm-based core/triple-shell nanophosphors for transparent displays," *Chemistry of Materials*, vol. 30, no. 23, pp. 8457–8464, 2018.

[47] Y.-P. Du, Y.-W. Zhang, L.-D. Sun, and C.-H. Yan, "Optically active uniform potassium and lithium rare earth fluoride nanocrystals derived from metal trifluroacetate precursors," *Dalton Transactions*, no. 40, pp. 8574–8581, 2009.

[48] M. R. Jones, K. D. Osberg, R. J. Macfarlane, M. R. Langille, and C. A. Mirkin, "Templated techniques for the synthesis and assembly of plasmonic nanostructures," *Chemical Reviews*, vol. 111, no. 6, pp. 3736–3827, 2011.

[49] J. Xie, X. Xie, C. Mi et al., "Controlled synthesis, evolution mechanisms, and luminescent properties of ScF_x:Ln (x = 2.76, 3) nanocrystals," *Chemistry of Materials*, vol. 29, no. 22, pp. 9758–9766, 2017.

[50] H. Dong, L. D. Sun, W. Feng, Y. Gu, F. Li, and C. H. Yan, "Versatile spectral and lifetime multiplexing nanoplatform with excitation orthogonalized upconversion luminescence," *ACS Nano*, vol. 11, no. 3, pp. 3289–3297, 2017.